Journal of Japan Association for Earthquake Engineering, Vol. 22, No. 3, 2022

RELATION BETWEEN H/V SPECTRUM RATIO OF MICROTREMOR AND THICKNESS OF SEDIMENTARY LAYER WITH DIFFERENT LANDFORM EVOLUTION: A STUDY FOR APPLYING MICROTREMOR TO HAZARD MAPS

Tsutomu OCHIAI[1], Takahisa ENOMOTO[2] and Iware MATSUDA[3]

[1] Member, Dr. Eng., Research Associate, Department of Architecture and Building Engineering, Kanagawa University, Kanagawa, Japan, ochiai@kanagawa-u.ac.jp
[2] Member, Dr. Eng., Professor, Department of Architecture and Building Engineering, Kanagawa University, Kanagawa, Japan, enomot01@kanagawa-u.ac.jp
[3] Dr. Sc., Professor Emeritus, Kantogakuin University, Kanagawa, Japan, iwr-maatsuda@fan.hi-ho.ne.jp

ABSTRACT: This study summarizes the predominant periods of the H/V spectral ratio of microtremors and sedimentary layer thicknesses above the engineering bedrock using topographic locations with varied landform evolution as objectives. The derived regression equation was unique to each location, indicating the evolution of the landform. Using the regression equation and earthquake observation data, we estimated the values of the ground's predominant period, which were consistent with the actual measured values. This result confirmed the significance of topographic classification. When creating ground hazard maps, the hazard-prone area should be classified into topographic areas based on the landform evolution as the basic information for the zoning. Then, these topographic areas should be further classified based on the H/V spectral ratio of microtremors and sedimentary layer's thickness.

Keywords: *Microtremors, H/V spectral ratio, Predominant period, Sedimentary layer thickness, Landform evolution*

1. INTRODUCTION

It is well known that the susceptibility of the ground to shaking varies according to the formation process and topographic variations in the landform[1), 2)]. Thus, earthquake hazard maps use topographic data and other information to analyze the ground from a seismic engineering perspective, with themed maps showing the ground susceptibility to shaking and vulnerability to liquefaction and slope failures. Boring surveys are typically used to collect ground information. However, in places where boring data is scarce, microtopography is frequently used as the primary source of information. The Cabinet Office (disaster

management) proposed using microtopography to obtain AVS30 (mean S-wave velocity from the ground surface to the depth of 30 m) for preparing "Earthquake Disaster Hazard Maps" across Japan[3]. Microtopographic data published by the National Research Institute for Earth Science and Disaster Resilience (NIED) is based on consistent nationwide data[4], and AVS30 obtained from such data are well suited to obtain a rough idea of the ground information from a wide area. AVS30 obtained from microtopography, on the other hand, shows more variations[5]; thus, it is suitable for acquiring a basic understanding of the entire country but not sufficiently accurate to understand seismic characteristics of local places like municipalities.

The use of microtremors is beneficial for making a detailed evaluation of ground vibrations in small areas. In particular, single-point ground surface observations can be made easily in a short period; thus, several studies conducted in the past have used microtremors[6, 7]. Several points need to be considered when evaluating the ground using the H/V spectral ratio (hereafter referred to as MHVR) from single-point observation of microtremors, such as foundation amplification characteristics[8], the basic mode of the Rayleigh wave[9], the use of diffuse-field theory[10, 11], and the type of waves, i.e., surface and body waves[12]. However, all approaches have one thing in common: the ground structure of the surface layer around the observation point has an impact. Various studies using microtremors are investigating these MHVR characteristics: one study found that stable ground vibrations could be roughly evaluated independently of temporal variations[13], another study estimated the spectral amplification factor from MHVR[14], and a third study evaluated the risk of direct ground shaking[15]. Other studies derive bedrock thickness from MHVR[16, 17], where areas are classified in the same way as in the current study (based on microtopography) and bedrock thickness is obtained from the predominant period[18]. The current authors investigated the construction of hazard maps using the predominant period and its peak value (amplification factor) where local characteristics are taken into consideration, confirming its effectiveness[19]. At the same time, it was confirmed that when the predominant period of MHVR for each microtopography result is summarized, variations within the same microtopography became larger than variations between different microtopography.

Ground vibration characteristics obtained from MHVR, such as the predominant period, do not always correspond to microtopography. This is because the actual landform borders and mesh boundaries may not be consistent, and microtopography may not accurately reflect the ground structure. In other words, microtopography is the final stage of landform evolution, and the ground formation process up to that point (i.e., landform evolution) is not always reflected.

Because landform evolution is the formation history of the ground, it appears as different thicknesses and properties of the bedrock, significantly contributing to the different vibration characteristics of the ground surface. The authors believe that by considering this landform evolution, variations in MHVR can be reduced, and by estimating the bedrock thickness from MHVR, hazard maps that precisely reflect local ground vibration characteristics can be generated. Thus, using the City of Yokohama (including a part of the City of Kawasaki) as our target, we identified four topographic areas with different landform evolutions—lowland created by small to medium rivers, lowland created by large rivers, loamy plateaus created by the sea, and loamy plateaus created by rivers—and summarized the relationship between the predominant period of MHVR and the thickness of the sedimentary layer above the engineering bedrock (hereafter referred to as sedimentary layer thickness) for each topographic area and showed different regression equations (regression coefficients of α, β) for each topographic area. Furthermore, we validated its applicability using actual earthquake records. We focused on the predominant period of MHVR because, in estimating seismic disasters in urban areas and analyzing damage of low to medium buildings in a case of massive earthquake further away, damage explained by the vibration of the ground surface layer is especially important[20].

2. TOPOGRAPHY AND BEDROCK OF THE TARGET AREAS

2.1 Summary of landform evolution

Figure 1 shows the surface geology of the survey target area[21]. The topography of the eastern part of

the Kanagawa prefecture, the study target, is roughly divided into lowlands, plateaus, and hills. These landforms reflect crustal movements, glacial eustasy, and volcanic ash supplied by Mount Hakone and Fuji in the west[22]. The hills are covered by Tama Loam, located in the southern part of Tama Hills, consisting of middle pleistocene sediments older than the last interglacial. Their elevations are higher than 60 m, with the hills are being dissected by valleys. Plateaus are divided into two types. A summary of the landform evolution is presented below and in Section 2.2; for details, refer to the literature[22].

The Shimosueyoshi Plateau, which is covered by the Shimosueyoshi Loam, is a landform developed from the former Tokyo Bay during the last interglacial 120,000 to 130,000 years ago. The period following this is known as the Late Pleistocene. Elevations of the plateau range from 40 to 60 m, and the plateau is dissected by small valleys and has more flat areas than in Tama Hills. The plateau covered by Musashino Loam is the Musashino Platea, which originated from lowland of an alluvial fan that was formed by the Sagami River as the sea level dropped during the last interglacial. Emerging about 100,000 years ago, it is covered by Kanto Loam, which is younger than the Shimosueyoshi Plateau.

The climate continued to cool until the last interglacial reached its apex around 20,000 years ago. The sea level dropped, Tokyo Bay became land, and vast valleys developed. The lowlands were created when valleys filled up to that point. Drowned valleys emerged in the survey area roughly 7,000 years ago during the Jomon Transgression's high sea level. It created a long, narrow inlet, which was buried to make way for lowlands. Through reclamation, most downstream area became land.

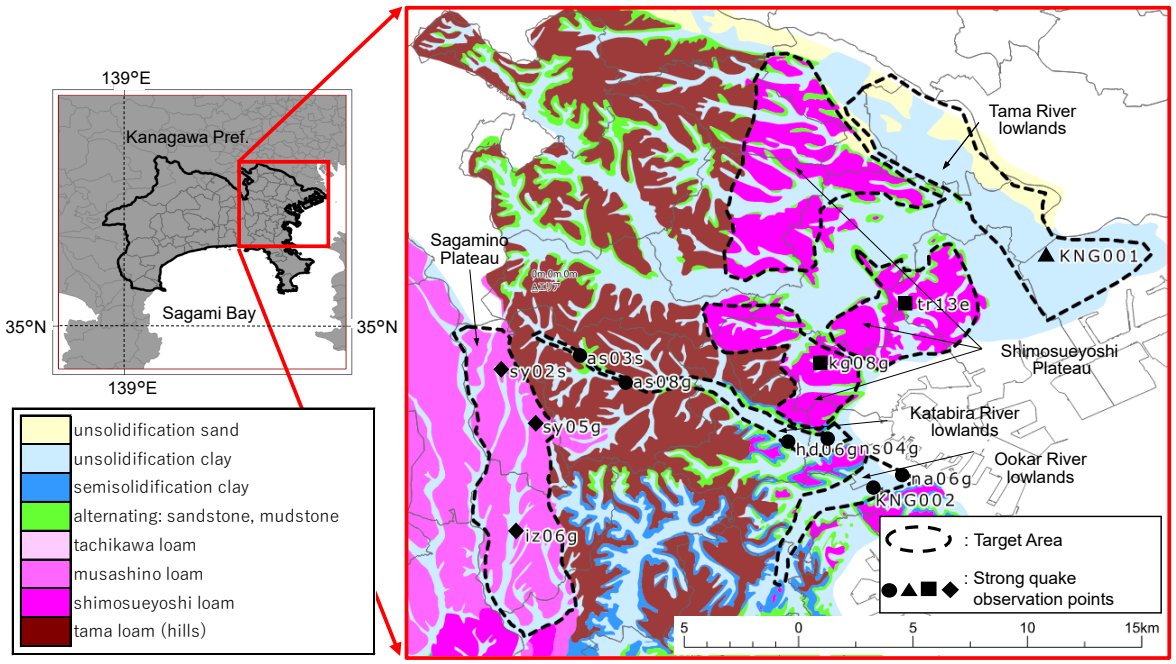

Fig. 1 Surface geology of the target area[21]

2.2 Bedrock of the survey area

2.2.1 Target topographic areas

The topographic areas in this paper were as follows: the Tama River lowland created by large rivers (hereafter referred to as the Tama River lowland), lowlands created by small and medium rivers, the Katabira River/Ooka River, the Shimosueyoshi Plateau created by the sea, and the Sagamino Plateau created by the river. The hills in the City of Yokohama are highly influenced by artificial creation and are thus unsuitable for studying landform development; thus, they were eliminated. The landform and bedrock of the Tsurumi River Lowland are very similar to those of the Katabira River/Ooka River; thus, they were excluded from the study.

By crustal movement and glacial eustasy, the landform was separated into plateaus and lowland. The

lowland was created when valleys built by the last interglacial's apex were buried as the sea level rose because of the subsequent warming. This is a common process in lowlands, but the manner of burial depends on each river's reaction to rising sea levels particularly, the sediment supply from the basin, different ability of rivers to transport sediment, whether they are facing an inner bay or an open ocean, and so on, which leads to different sediment (bedrock)[23]. Because plateaus are elevated lowlands, their bedrock structure is based on the landform evolution of the original lowlands.

Sediment above the engineering bedrock is highly significant when preparing a bedrock hazard map and estimating seismic damage; hence, we defined sediment above the engineering bedrock as the sedimentary layer, which is the study goal. Figure 2 shows the representative log for each topographic area[24), 25)], and Table 1 shows the landform, engineering bedrock, and sedimentary layer[20), 21)]. The S-wave velocity of the engineering bedrock (hereafter referred to as *V*s) was obtained from the PS logging sites of Chapter 5. It was around 400 m/s for all four areas, similar to engineering bedrock for construction. In general, sediment from the climax of the last interglacial is defined as alluvium[26)]. This study focuses on the sediment layer in the lowlands. We present the mean Vs calculated weighting the sedimentary layer with the layer thickness; however, this is mainly for reference because the mean was obtained from a few points.

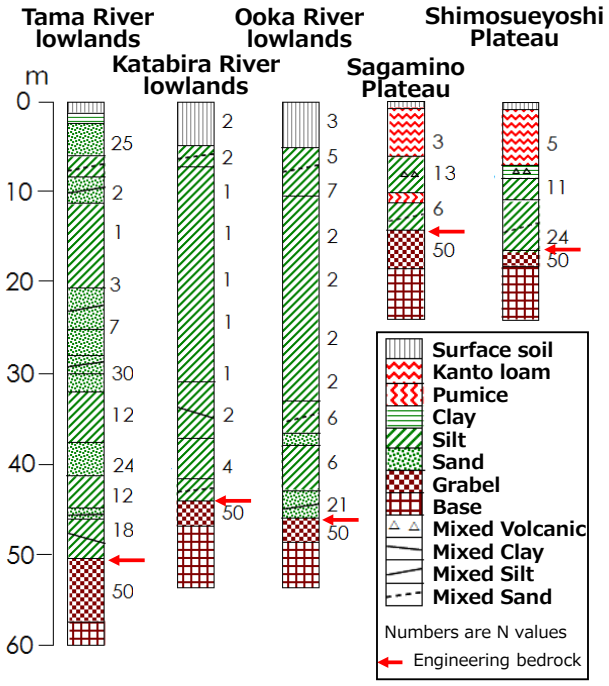

Fig. 2 Representative logs of the target [24), 25)]

Table 1 Landform, engineering bedrock, and a sedimentary layer of the target area[22), 27)]

Area	Landform	Engineering bedrock		Sedimentary layer			
		Layer	Vs (m/s)	Era	Soil layer	N value	Average Vs(m/s) ( ) is number
Tama River lowlands	River plain	Alluvium base rock Middle Pleistocene	400	Alluvium	Upper：clay・silt	2～5	137 (1)
					Lower：sand・clay・silt alternate layers	10～15 (clay)	
						20～30 (sand)	
Katabira River and Ooka River lowlands	River plain	Middle Pleistocene	425	Alluvium	Upper：clay・silt	0～3	114 (6)
					Lower：clay・silt	5～12	
Shimosueyoshi Plateau	Loam plateau (formed by the sea)	Middle Pleistocene	445	Kanto loam new pleistocene	Kanto loam	5～10	142 (2)
					sand・clay・silt	6～15 (clay)	
						around 20 (sand)	
Sagamino Plateau	Loam plateau (formed by the river)	Sagamino gravel	435	Kanto loam new pleistocene	Kanto loam	2～12	185 (3)
					clay・silt	2～15	

2.2.2 The Tama River lowlands and the lowlands of Katabira River/Ooka River[22), 27)]

The Tama River lowlands and the Katabira River and Ooka River lowlands originated when valleys carved by the culmination of the last interglacial became drowned valleys that were later submerged. The engineering bedrock in the Tama River lowland is the basal gravel layer of an alluvial fan at the valley's base. Middle Pleistocene deposits become the engineering bedrock where this gravel layer does not exist. A sand layer with an N value of about 30 at a depth of about 30 m exists in the Tama Lowland, which was created by a big river. This sand layer comprises sediments from the Younger Dryas period (the final stadial interval that separates the Late Pleistocene and Holocene epochs), and it is separated into upper and lower sections. The lower alluvium is made up of alternating layers of sand with a high N value deposited on a floodplain and clay/silt. The higher alluvium is made primarily of clay and silt deposited in the Jomon Transgression inlet. The topmost layer contains sediment from the delta that covered the inlet. The sediment from the river that forms the microtopography is found above this sand layer.

The Katabira River/Ooka River lowlands contain a thin base gravel alluvial layer, and the engineering bedrock is typically the Middle Pleistocene deposit underneath. The alluvium contains little sand and has an N value of five or above. The Younger Dryas or older floodplain deposit is thin. The Jomon Transgression inlet's sediment is thick, with a dominant weak clay and silt layer with small N.

2.2.3 Shimosueyoshi Plateau and Sagamino Plateau[22), 27)]

The Shimosueyoshi Plateau and the Sagamino Plateau are both loam plateaus. However, the Shimosueyoshi Plateau was formed by the sea when shallow seafloor emerged during the last interglacial's climax, whereas the Sagamino Plateau was formed by the river when alluvial fan lowlands formed during the last interglacial were terraced. Their sedimentary environment and emergency era are not the same. The Middle Pleistocene deposit serves as the basic bedrock for the Shimosueyoshi Plateau, with the Late Pleistocene deposit (the Shimosueyoshi layer) and the underlying Kanto Loam serving as the primary sedimentary strata. The deposit comprises alternating layers of sand, silt, and clay from the Late Pleistocene period. The places that were valleys during the preceding glacial epoch have thick distribution, whereas the areas that were wave-cut platforms have thin distribution.

The river gravel layer that forms the plateau (Sagamino gravel layer) is the engineering bedrock of the Sagamino Plateau, whereas the sedimentary layers are clay and silt that formed during emergence and the underlying Kanto Loam. The Kanto Loam is thinner than the Shimosueyoshi Plateau due to its later era of emergence.

3. MIROTREMORS OBSERVATIONS

3.1 Observation and analytical methods for microtremors

Since the 1990s, the authors continuously observed high-density microtremors around Kanagawa Prefecture[28), 29)]. The authors examine the ground vibration characteristics of each city in eastern Kanagawa Prefecture by observing the center of a 250 × 250 m mesh. We used part of the data in the present study.

The observation was performed with two horizontal components (EW and NS components) and one vertical component (UD component), where sampling was done every 180 s at 100 Hz. Table 2 shows the properties of the microtremor measurement device used for the observation[19)]. Microtremor observation used three types of microtremor measurement devices, A, B, and C, depending on the timing of the measurement. A huddle test was performed as needed between these observation devices. We confirmed that there is hardly any difference between devices in the periodic band targeted in this study (0.1 to 2.0 s).

We identified numerous steady intervals (2,048 points) with relatively low noise from the waveform of three observable components and calculated the Fourier spectrum. The Fourier spectrum is smoothed using a Parzen window with a bandwidth of 0.3 Hz. A geometric mean was derived for the spectra of the two horizontal components at each interval, and the MHVR was calculated by dividing by the UD component. Finally, the MHVR of the detected periods was averaged, and the dominating period was read. We selected a period with an MHVR of at least two to read the dominant period. We decided if several peaks could be confirmed based on the observation results and ground structure of the surrounding areas. Figure 3 shows a microtremor observation record as well as an example of the spectrum.

Table 2 A list of microtremor observation devices used[19)]

<table>
<tr><th></th><th>A</th><th>B</th><th>C</th></tr>
<tr><td>Recorder</td><td>SPC-35</td><td>SPC-51</td><td>JU410</td></tr>
<tr><td>Amp</td><td>Tokyo Sokushin</td><td>Tokyo Sokushin</td><td>Hakusan kougyou</td></tr>
<tr><td>Sensor</td><td colspan="2">VSE-15D
Tokyo Sokushin
Velocity sensor
Frequency characteristic：
0.2–10.0 Hz</td><td>（Recorders, amplifiers, One sensor）
Accelerometer
Frequency characteristic：
0.2–10.0 Hz</td></tr>
</table>

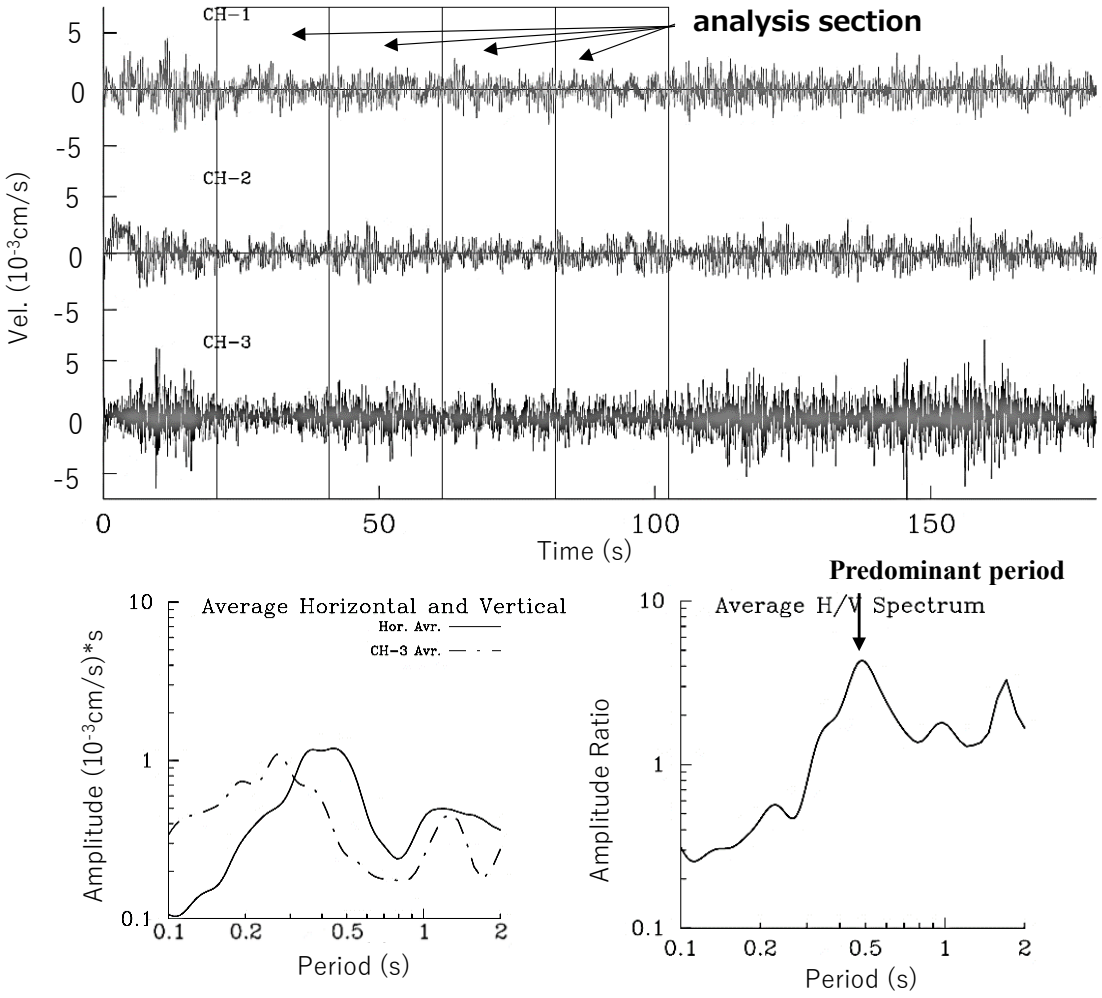

Fig. 3 An example of microtremor observation data and analytical result

3.2 Predominant period distribution of microtremors

Figure 4 shows the distribution of the predominant period obtained from MHVR for the eastern Kanagawa Prefecture. The prominent period was the longest in the current target topographic areas in the downstream area of the Katabira River and Ooka River lowlands, where there were several places with a predominant period of 1 s or longer. The Tama River lowland's dominant period saw slight variation between downstream and upstream locations, with values ranging between 0.5 and 0.8 s overall. The predominant period of the Shimosueyoshi Plateau was roughly 0.3 to 0.8 s; points with a comparatively long predominant period were located in small valleys that dissect in a dendritic manner. The predominant period of the Sagamino Plateau was often 0.3 s or less.

Though not the focus of this study, the Tsurumi River lowland, which cuts through the Shimosueyoshi Plateau, features points where the predominant period is 1 s or longer, similar to the Katabira River/Ooka River lowland. This is because the clay deposit similar to the lowland of Katabira River/Ooka River is dominant. The predominant period of the hills where the Tama Loam is widely distributed is frequently 0.3 s or shorter in the north of the Katabira River Lowland and 0.3–0.8 s in the south, which is slightly longer. The reason for this is likely the impact of topographic changes associated with different thicknesses of Tama Loam and large-scale landform creations[22], but this is outside of the scope of this study.

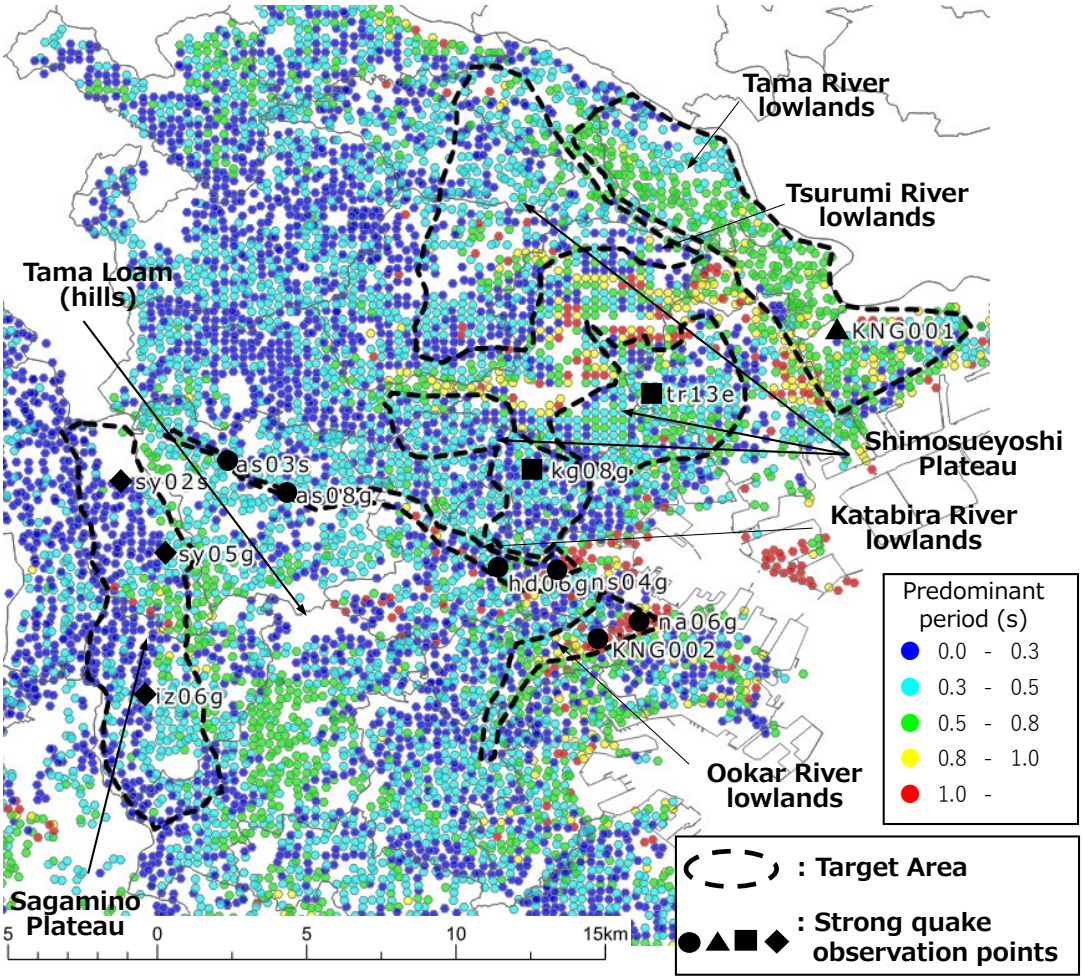

Fig. 4 The predominant period distribution of MHVR

4. THE RELATIONSHIP BETWEEN BEDROCK THICKNESS AND PREDOMINANT PERIOD

4.1 The relationship between sedimentary layer thickness and predominant period

We read the thickness of the sedimentary layer from the boring log summarized by the City of Yokohama[30], summed the relationship with the predominant period, and obtained the regression equation. The regression equation was transformed into a linear regression Eq. (1), with a coefficient α where the unit thickness of the sedimentary layer contributes to the predominant period and a coefficient β that cannot be explained by the thickness. If $\beta = 0$, theoretically, $\alpha = 4/ V_s$ because of the quarter wavelength rule ($T = 4H/V_s$); however, in reality, β might not be 0. β is a constant term generated by linear regression, related to the residual difference after regression. Though the regression coefficient β is reported as a single number for simplicity, in reality, there are multiple implications such as underground structures below the engineering bedrock and modeling of the sedimentary layer.

$$T_0 = \alpha \times H + \beta \tag{1}$$

For boring logs to read layer thickness, we examined topography and elevation and chose data within 100 m of the microtremor observation points to assume the same sedimentary layer. In other words, our investigation includes mistakes in bedrock thickness caused by differences in boring points and

microtremor observation points. To eliminate false variations in thickness, we chose data from places with the fewest artificial adjustments for plateaus. For hills, we omitted data from developed land that had undergone significant modification. We eliminated data from landfills in coastal areas.

First, we used the complete dataset without taking into account the topographic areas to describe the association between sedimentary layer thickness and the predominant period. The outcome is depicted in Fig. 5 and Eq. (2).

$$T_0 = 0.018 \times H + 0.180 \, (R = 0.73, n = 255) \tag{2}$$

T_0: predominant period (s), H: sedimentary layer thickness (m), n: number of data,
R: correlation coefficient, α, β: regression coefficient (common for Eqs. (1)–(11))

Generally, when the thickness of the sedimentary layer increased, the predominant period increased in a positive correlation. The correlation coefficient is not poor, although there are notable differences. Figure 6 shows the predominant period and sedimentary layer thickness for points where PS logging was performed based on the whole dataset (see Figs. 1 and 4). Though the amount of data is limited, we obtained regression equations for small and medium rivers of lowlands (T_{0A}) and loam plateaus formed by rivers (T_{0D}) and displayed these together. The regression coefficient α was large for lowlands and small for loam plateaus. In the next Section, we increased and reorganized data for four topographic areas with different landform evolutions.

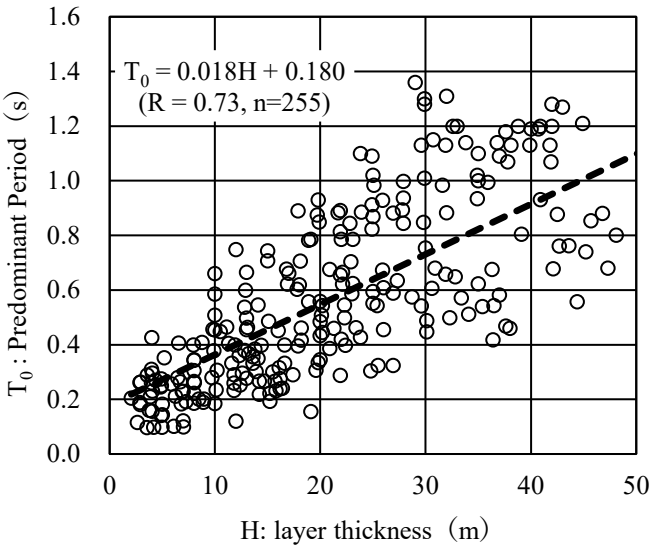

Fig. 5 Relationship between sedimentary layer thickness and predominant period

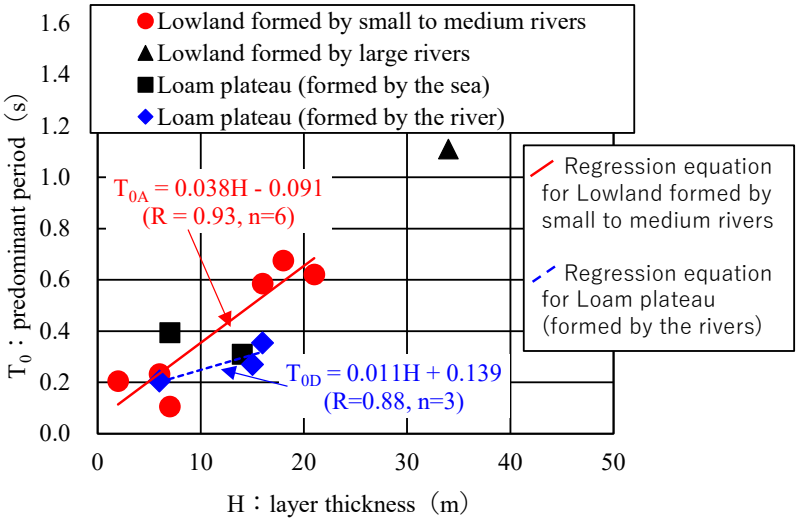

Fig. 6 Relationship between sedimentary layer thickness and predominant period at PS logging points

4.2 Relationship between sedimentary layer thickness and predominant period for each topographic area

Figures 7(a) and (b) show the relationship between the sedimentary layer thickness and predominant period for the Katabira River and Ooka River lowlands. Equations (3) and (4) show the regression equations. The value of regression coefficient α was consistent, and the correlation coefficient R was high for each at 0.91, which is a coincidence. Both lowlands are close and of similar size, having similar landform evolutions. Thus, we combined them in subsequent discussions.

The Tama River lowland result is shown in Fig. 7(c) and Eq. (5). The thickness of the sedimentary layer and the predominant period have a strong correlation. However, the slope of the regression equation, α, was smaller than the two rivers discussed above. In other words, contribution by a unit sedimentary layer thickness to predominant period is small. As discussed in Section 2.2, this is because their landform evolution is different, and the geology of sedimentary layer is also different.

$$\text{Katabira River Lowland } T_0 = 0.030 \times H + 0.072 \, (R = 0.91, n = 54) \tag{3}$$

$$\text{Ooka River Lowland } T_0 = 0.027 \times H + 0.158 \, (R = 0.91, n = 83) \tag{4}$$

$$\text{Tama River Lowland } T_0 = 0.013 \times H + 0.160 \, (R = 0.87, n = 57) \tag{5}$$

Figures 7(d) and (e) show the relationship between the Shimosueyoshi Plateau and the Sagamino Plateau. Their regression equations are shown in Eqs. (6) and (7). All results show a smaller slope α compared to the lowlands result, while β is larger. The correlation coefficient was low. These results are consistent with the trend seen in the result that used PS logging (Fig. 6). S wave velocity of the engineering bedrock is similar for plateaus and lowlands (see Table 1); thus, the small α likely reflects the difference in the S-wave velocity of the sedimentary layers. As previously discussed, multiple impacts of different β are feasible; however, its constant term of regression equation is beyond the scope of the current dataset (extrapolation portion).

$$\text{Shimosueyosi Plateau } T_0 = 0.007 \times H + 0.239 \, (R = 0.56, n = 34) \tag{6}$$

$$\text{Sagamino Plateau } T_0 = 0.004 \times H + 0.228 \, (R = 0.35, n = 27) \tag{7}$$

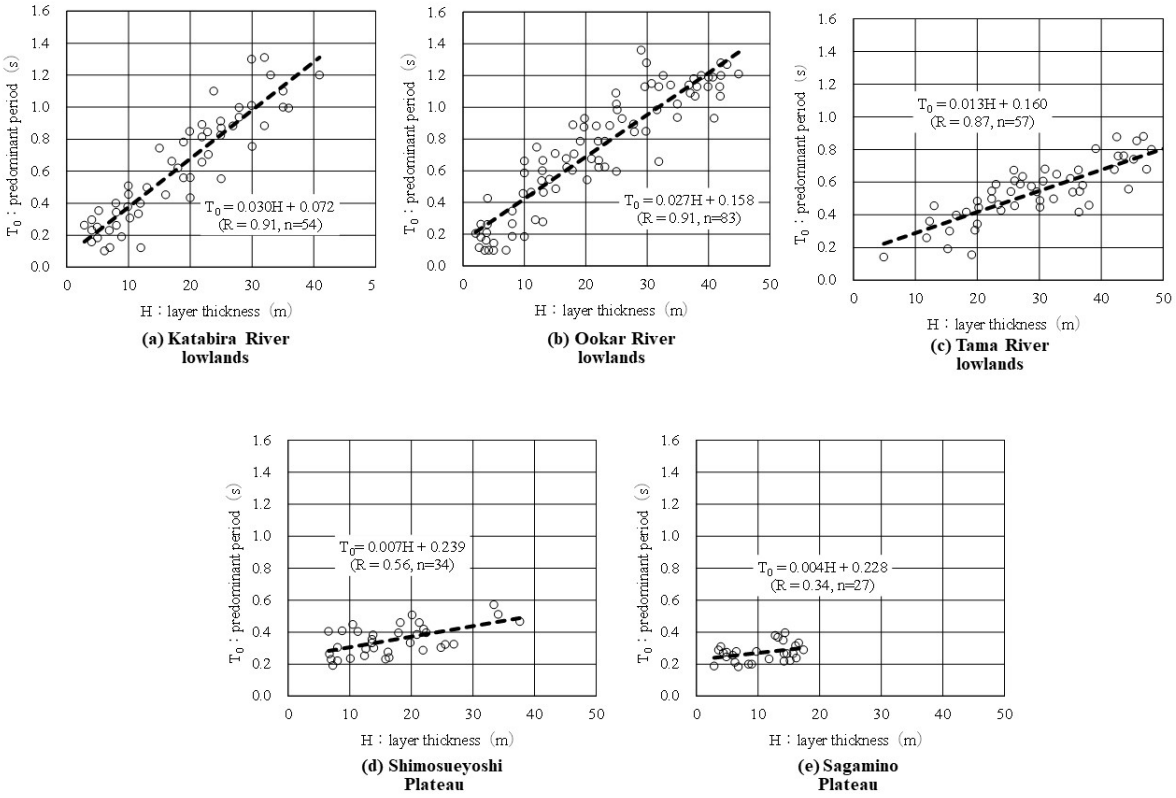

Fig. 7 The relationship between sedimentary layer thickness and predominant period for each topographic area

4.3 Reorganization of the relationship between sedimentary layer thickness and predominant period for each topographic area

We observed in the previous Section that the Katabira River lowland and the Ooka River lowland were both lowlands formed by minor rivers and had similar bedrock formations during their landform evolution. We integrated them since their regression equations were comparable, as shown in Fig. 7.

The Shimosueyoshi Plateau and Sagamino Plateau were both classified as loam plateaus, and although they share a small α and a large β. However, a differs by a factor of 2, and the process of bedrock formation (topographic evolution) is also different. As a result, we employed various regression equations for them (Eqs. (8) to (11) and Fig. 8).

Let us analyze the relationship between the sedimentary layer thickness and predominant period with prior studies. In a previous study of the Sagami River basin [28], α was 0.014 (sandy bedrock) and 0.024 (clay bedrock), which is similar to the Tama River lowland. Toshinawa et al.[17] summarized the upstream area of Tsurumi River in the City of Yokohama in a similar manner and found the regression coefficient α to be 0.056 (since the definition of regression coefficient in the paper was different, we recalculated with our definition). The four topographical areas of the present study are closest to the cases involving small and medium rivers, which is consistent with the present result. Since topography has dramatic variations along the coast of Japan, comparison is difficult; however, Kojima et al.[19] analyzed the relationship between alluvial thickness and period of the Fukui Plain based on microtopography. The result showed a similar linear regression trend, but the correlation coefficient ranged between R of 0.43 and 0.85. Thus, our alluvial result that considered landform evolution had a higher correlation (lowlands formed by small, medium, and large rivers).

Lowland formed by small to medium rivers

$$T_0 = 0.028 \times H + 0.127 \ (2 \leq H \leq 45) \ (R = 0.91, n = 137) \quad (8)$$

Lowland formed by large rivers

$$T_0 = 0.013 \times H + 0.160 \ (5 \leq H \leq 50) \ (R = 0.87, n = 57) \quad \text{Eq. (5) reposted} \quad (9)$$

Loam plateau (formed by the sea)

$$T_0 = 0.007 \times H + 0.239 \ (7 \leq H \leq 40) \ (R = 0.56, n = 34) \quad \text{Eq. (6) reposted} \quad (10)$$

Loam plateau (formed by the rivers)

$$T_0 = 0.004 \times H + 0.228 \ (3 \leq H \leq 17) \ (R = 0.34, n = 27) \quad \text{Eq. (7) reposted} \quad (11)$$

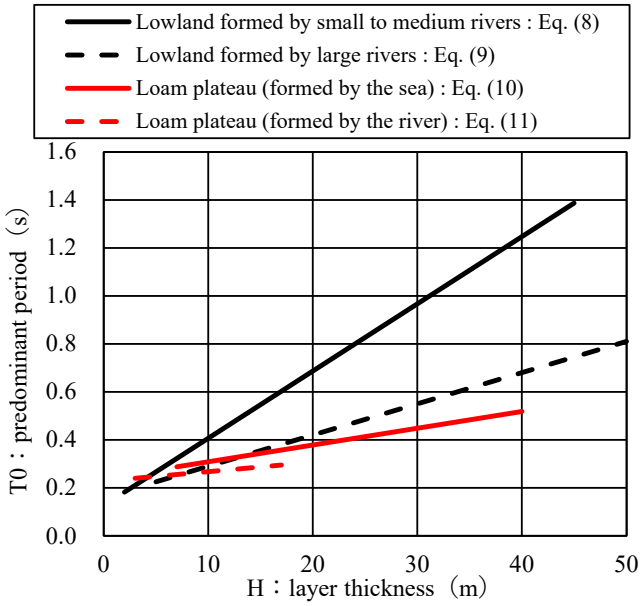

Fig. 8 Relationship between sedimentary layer thickness and predominant period for each topographic area reorganized

5. CONFIRMATION BY OBSERVATION RECORD OF EARTHQUAKES

5.1 Record of earthquakes used for the examination

In this study, we determined whether actual seismic properties in strong quake observation points with known sedimentary layer thickness are consistent with regression equations. The examination points consisted of 12 points from the Yokohama City Strong-Motion Network[31] and K-NET[32] that were located within the target topographic areas (see Figs. 1 and 4). The breakdown is as follows: Six points in lowlands formed by small and medium rivers, one point in lowlands formed by a large river, two points in loam plateaus (by the sea), and three points in loam plateaus (by rivers). For the name of the observation points, we used the names from the Yokohama City Strong-Motion Network and K-NET. Five significant earthquakes were selected from strong quakes observed between 2012 and 2018 (about 270 quakes). We assumed vertical propagation from below for all observation points and used the following conditions 1 to 3 for the selection of said five earthquakes. The maximum acceleration of the selected earthquakes was about 100 cm/s^2. Table 3 shows the list of earthquake records.

1. Relatively large earthquakes of *M* (magnitude) 4.5 or higher
2. Earthquakes with the epicenter depth of 30 km or more
3. Earthquakes that were recorded at almost all observation points

We performed Fourier transform on the earthquake records including the main motion (60 s from the start of the record) and smoothed in the same manner as the microtremor record in Section 3.1 (Parzen window with a bandwidth of 0.3 Hz). The H/V spectral ratio was calculated by dividing the geometric mean of two horizontal components by the vertical component (hereafter referred to as EHVR). Figure 9 shows an example of observation records (point: KNG002, time: 2014/5/5 5:18). All earthquakes stopped within 60 s, which confirms that when EHVR is calculated using the coda part of seismic motion it provides a similar trend to the present interval[19].

Table 3 A list of strong quake records for the examination

No.	Time of occurrence	Epicentral location		Depth	Scale
		Lat.	Lon.	(km)	M
1	2012/11/24 17:59	35.64	140.20	72	4.8
2	2013/4/14 10:22	36.00	139.50	97	4.6
3	2014/5/5 5:18	34.95	139.48	156	6.0
4	2014/9/16 9:16	36.90	139.86	47	5.6
5	2016/11/23 3:45	34.54	140.07	101	4.5

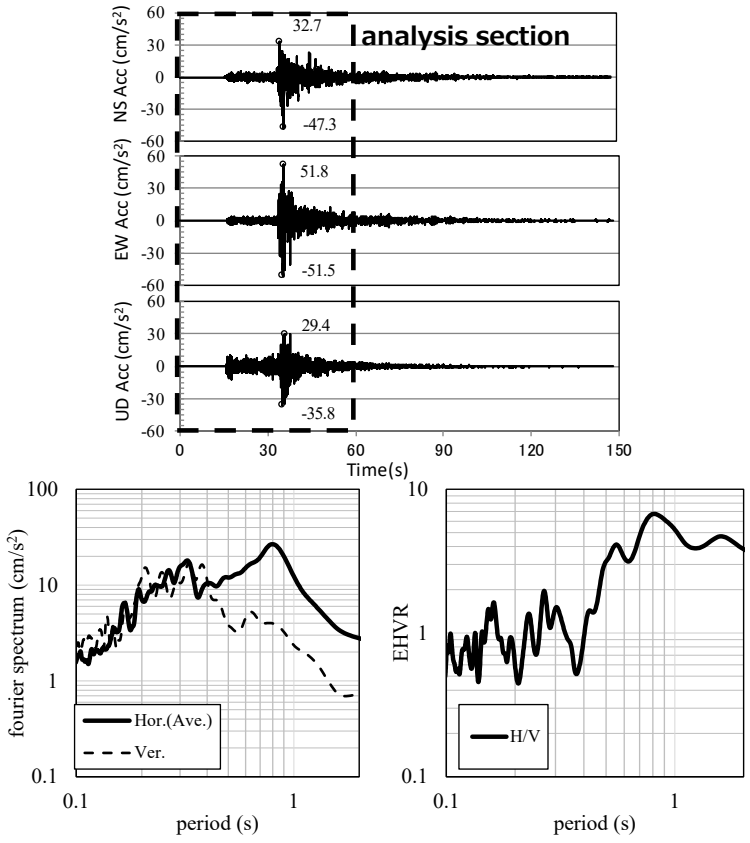

Fig. 9 Record of strong quake observations and analytical results (KNG002, 2014/5/5)

5.2 Relationship between ground amplification properties and sedimentary layer thickness

Figure 10 shows the calculated EHVR. The figure shows the EHVR of each earthquake and the mean. Generally, each quake and the mean overlap. Thus, we assumed that the mean EHVR represents the seismic characteristic of each point and read its predominant period (shown with ↓ in the figure).

However, we estimated the predominant period of the bedrock using sedimentary layer thickness of each point and Eqs. (2), and (8) to (11). The sedimentary layer thickness was read from boring data published for each point[30), 32)]. Additionally, KNG001 did not reach the engineering bedrock in the bedrock data from K-NET; thus, we set the sedimentary layer thickness by assuming that the depth at which V_s becomes 400 m/s as the engineering bedrock based on the nearby boring data and underground structural model of the seismic headquarter[33)].

Figure 11 shows the result of the comparison. The horizontal axis shows the predominant period determined using the microtremor observation regression equation. The vertical axis represents the dominating time as determined by the seismic observation record. It also displays the estimates from regression Eqs. (8) to (11) for each topographic area, as well as the overall data estimates from regression Eq. (2). Estimates using regression equations of each topographic area are more consistent to the main period of the powerful seismic observation record than estimates from the entirety of the data. This demonstrates that the predominant period determined by the regression equations and reexamined by topographic areas is more consistent with the predominant period determined by the strong quake observation record.

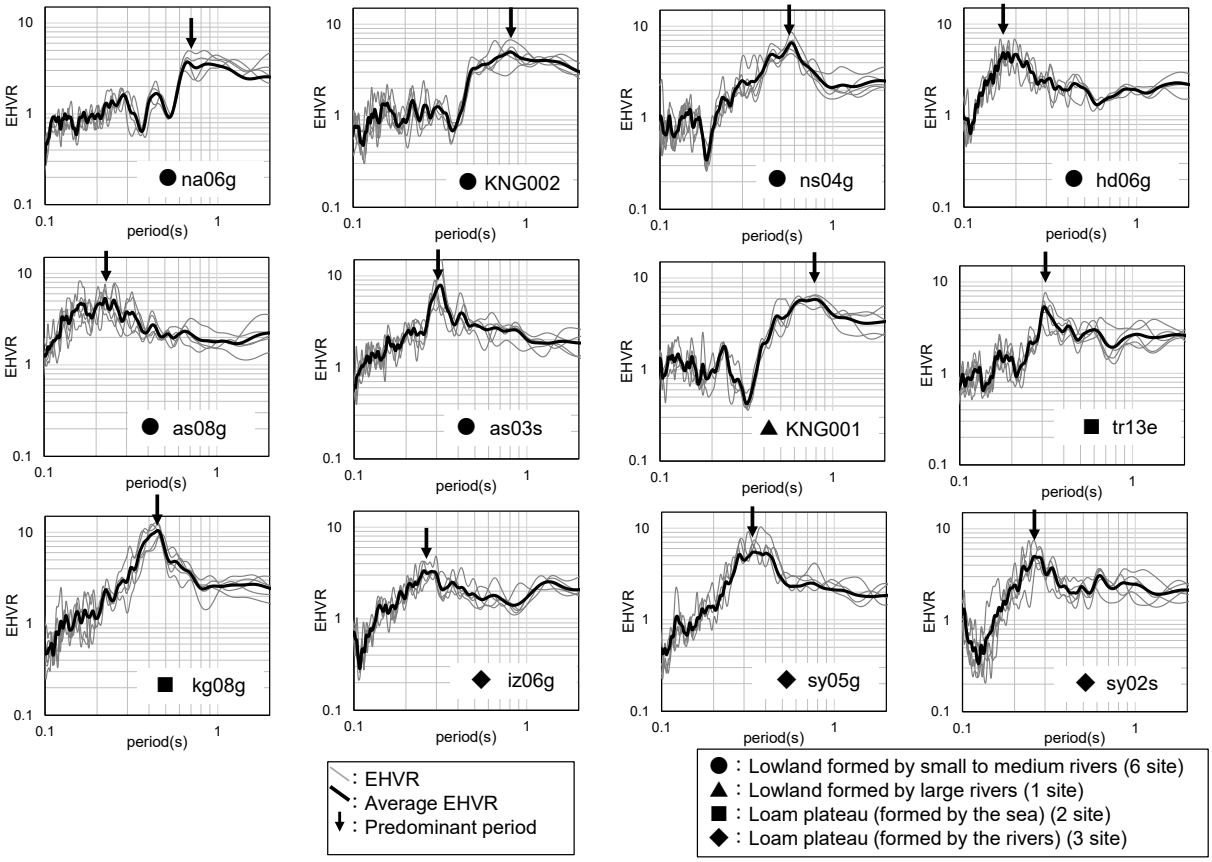

Fig. 10 EHVR and mean EHVR of strong quake observation record for each earthquake

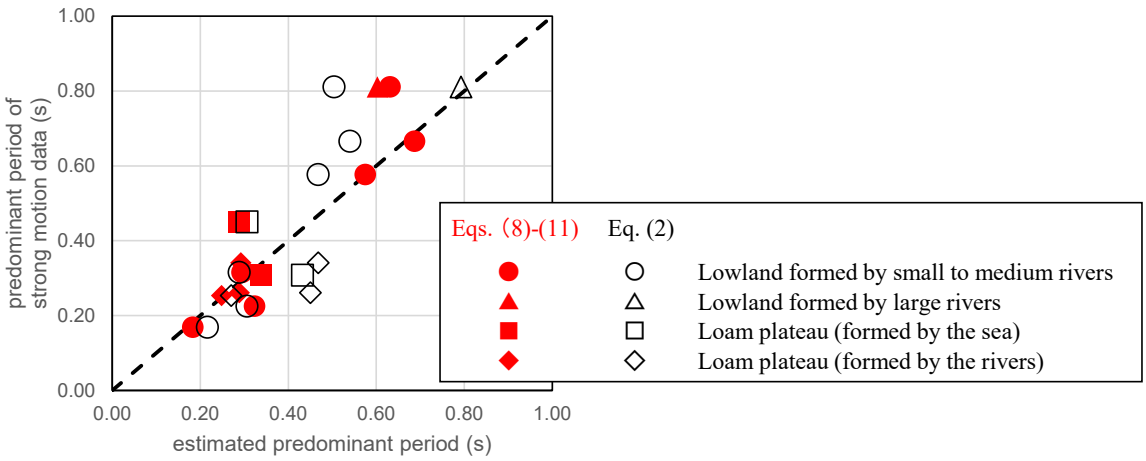

Fig. 11 Relationship between predominant period estimated from sedimentary layer thickness and predominant period of strong quake record

6. SUMMARY

In this paper, we calculated the predominant period of MHVR for four topographic areas in the City of Yokohama (including parts of the City of Kawasaki) with different landform evolutions (i.e., lowlands formed by small to medium rivers, lowlands formed by large rivers, loam plateaus formed by the sea, and loam plateaus formed by rivers) and showed the relationship between the predominant period and the sedimentary layer thickness above the engineering bedrock using linear regression equations. The result showed that regression coefficients differed for each topographic area (α and β). For the obtained regression equations, we confirmed the validity using the actual strong quake observation records. The results are as follows:

1. The relationship between the predominant period of MHVR and the sedimentary layer thickness varies between topographic areas with different landform evolutions.
2. The values of α and β differ for lowlands and plateaus. The value of α is large for lowlands and small for plateaus, while the value of β is small for lowlands and large for plateaus.
3. The value of α for lowlands formed by small to medium rivers is clearly larger than lowlands formed by large rivers.
4. Though landform evolution of plateaus formed by rivers and formed by the sea is different, the value of α is small for both; thus, practically, these plateaus may be summarized as loam plateaus.
5. The predominant period estimated from the regression equations obtained for each topographic area through microtremor observations and sedimentary layer thickness was generally consistent with the predominant period of strong quake records. Thus, the use of microtremors for bedrock hazard maps is effective.

ACKNOWLEDGMENT

In the present study, we had the privilege to use the strong-motion seismograph networks (K-NET) of NIED and strong-motion observation network of the City of Yokohama. The microtremor observation data was obtained from the work of graduate students and postdocs of the Enomoto Laboratory of Kanagawa University. Specifically, Mr. Toshio Yamamoto (former assistant at Kanagawa University) and Dr. Tetsushi Inubushi (lecturer at Kindai University) provided tremendous support for observation planning and implementation. Here, we extend our most sincere appreciation.

REFERENCES

1) Matsuda, I.: Verifying Vulnerability to Natural Disasters in Tokyo, *Journal of Geography (Chigaku Zasshi)*, Vol. 122, No. 6, pp. 1070–1087, 2013 (in Japanese).
2) Kumaki, Y., Koarai, M. and Nakano, T.: Land Transformation in Tokyo and Its Surrounding Regions, *Journal of Geography (Chigaku Zasshi)*, Vol. 122, No. 6, pp. 992–1009, 2013 (in Japanese).
3) Cabinet Office (Disaster Prevention): Technical Data for Creating an Earthquake Disaster Prevention Map, 143 pp., 2005 (in Japanese, title translated by the authors).
4) Wakamatsu, K. and Matsuoka, M.: Nationwide 7.5-Arc-Second Japan Engineering Geomorphologic Classification Map and Vs30 Zoning, *Journal of Disaster Research*, Vol. 8, No. 5, pp. 904–911, 2013.
5) Matsuoka, M., Wakamatsu, K., Fujimoto, K. and Midorikawa, S.: Average Shear-wave Velocity Mapping Using Japan Engineering Geomorphologic Classification Map, *Journal of Japan Society of Civil Engineers*, Vol. 794/I-72, pp.239–251, 2005 (in Japanese).
6) Kagami, H.: Obsrvation of Microtremors and its Application to Earthquake Engineering, *Journal of Geography (Chigaku Zasshi)*, Vol. 97, No. 5, pp. 409–422, 1988 (in Japanese).
7) Horike, M.: Studies on Micotremors, *Jornal of the Seismological Society of Japan. 2nd ser.*, Vol. 46, 343–350, 1993 (in Japanese).
8) Nakamura, Y.: A Method for Dynamic Characteristics Estimation of Subsurface Using Microtremor on the Ground Surface, *Quarterly Report of RTRI*, Vol. 30, No.1, pp. 25–33, 1989.
9) Tokimatsu, K. and Tamura S.: Contribution of Rayleigh and Body Waves to Displacement Induced by A Vertical Point Force on A Layered Elastic Half-space, *Journal of Structural and Construction Engineering, Architectural Institute of Japan*, No. 476, pp. 95–101, 1995 (in Japanese).
10) Sanchez-Sesma, F. J., Rodrigues, M., Iturraran-Viveros, U., Luzon F., Campillo, M., Margerin, L., Garcia-Jerez, A., Suarez M., Santoyo, M. A. and Rodriguez-Castellanos, A.: A Theory for Microtremor H/V Spectral Ratio: Application for a Layered Medium, *Geophysical Journal International*, Vol.186, pp. 221–225, 2011.
11) Matsushima, S., Hirokawa, T., Martin, F. D., Kawase, H. and Sanchez-Sesma, F. J.: The Effect of Lateral Heterogeneity on Horizontal-to-Vertical Spectral Ratio of Microtremors Inferred from Observation and Synthetics, *Bulletin of Seismological Society of America*, Vol. 104, No. 1, pp. 381–393, 2014.
12) Nagao, T., Yamada, M. and Nozu, T.: A Study on the Interpretation of Wave Components in Microtremor H/V Spectrum, *Journal of Japan Society of Civil Engineers*, *Ser. A1*, Vol. 68, No. 1, pp.48–62, 2012 (in Japanese).
13) Motoki, K., Watanabe, T., Kato, K., Takesue, K., Yamanaka, K., Iiba, M. and Koyama, S.: Characteristics of Temporal and Spatial Variation in Peak Periods of Horizontal to Vertical Spectral Ratios of Microtremors—Case Study at Flat Engineering Bedrock Sites and Its Interpretation—, *Journal of Structural and Construction Engineering, Architectural Institute of Japan*, Vol. 81 No. 721, pp. 437–445, 2016 (in Japanese).
14) Senna S., Midorikawa, S. and Wakamatsu, K.: Estimation of Spectral Amplification of Ground Using H/V Spectral Ratio of Microtremors and Geomorphological Land Classification, *Journal of Japan Association for Earthquake Engineering*, Vol. 8, No. 4, pp. 1–15, 2008 (in Japanese).
15) Nakamura, Y., Hara, T. and Yamada, M.: Study on Risk Evaluation Method for Ground Shaking Hazard by Microtremor Observation, *Journal of Japan Society of Civil Engineers, Ser. A1*, Vol. 74, No. 4, pp. 675–685, 2018 (in Japanese).
16) Maeda, T. and Abeki, N.: Dynamic Characteristics of Surface Geology Estimated by Microtremors in Fukui Plain—The Correspondence with the Damage of the 1948 Fukui Earthquake—, *Journal of Social Safety Science*, No. 3, pp. 148–156, 2001 (in Japanese).
17) Toshinawa, T., Takahama, T. and Nakayama, M.: Subsurface-Soil Thickness in Ikonobe Area, Yokohama, Evaluated from Microtremor Observation, *Journal of Japan Association for Earthquake Engineering*, Vol. 20 No. 1, pp. 26–36, 2020 (in Japanese).

18) Kojima, K. and Yamanaka, H.: Estimation of Quaternary Structure of Fukui Plain Based on Microtremor Observation, *Journal of Japan Society of Civil Engineers*, Vol. 752/I-66, pp.217–225, 2004 (in Japanese).
19) Ochiai, T. Inubushi, T. and Enomoto, T.: Creation of a Hazard Map Considering Regional Characteristics by Microtremor, *Journal of Japan Association for Earthquake Engineering*, Vol. 19 No. 5, pp. 136–145, 2019 (in Japanese).
20) Matsuda, I., Wada, S. and Miyano, M.: The Relation Between Subsoil Condition and the Collapse Rate of Wooden Houses due to the Great Kanto Earthquake of 1923 in Yokohama City, *Journal of Geography (Chigaku Zasshi)*, Vol. 87, No. 5, pp. 14–23, 1978 (in Japanese).
21) Ministry of Land, Infrastructure, Transport and Tourism, MLIT: 1/200,000 Basic Land Information Classification Survey GIS Data, Surface Geological Map (Kanagawa), 1975 (in Japanese, title translated by the authors). https://nlftp.mlit.go.jp/kokjo/inspect/inspect.html (last accessed on February 2, 2022)
22) Kanto Branch of Japanese Geotechnical Society, Kanagawa Group: Ooinal Kanagawano Ziban, Gihodosyuppan, pp. 11–60, 2010 (in Japanese).
23) Umitsu, M.: Geomorphic Evolutions of the Alluvial Lowlands in Japan, *Geographical Review of Japan*, Vol. 54, No. 3, pp. 142–160, 1981 (in Japanese).
24) Yokohama City: Yokohama City Administrative Map Information Provision System Ziban View, 2022 (in Japanese). https://wwwm.city.yokohama.lg.jp/yokohama/Portal?mid=3 (last accessed on February 2, 2022)
25) Kawasaki City: Guide Map Kawasaki Geological Map Collection, 2022 (in Japanese, title translated by the authors). http://kawasaki.geocloud.jp/webgis/?p=1 (last accessed on February 2, 2022)
26) The Geological Society of Japan, Field Geology Publication Committee: Daiyonki, Kyoritushuppan, pp. 62–63, 2012 (in Japanese).
27) Matsuda, I.: Taiwademanabu EdoTokyo Yokohamanotikei, Chapter3, Chapter 8, Collegio, pp. 84–105, pp. 212–239, 2013 (in Japanese).
28) Ochiai, T., Yamamoto, T., Hattori, H. and Enomoto, T.: Study on Zoning for Ground Shaking Characteristics of Surface Soil Structure in Sagami Plain Using Spatially Dense Microtremor Measurements, *Journal of Social Safety Science*, No. 5, pp. 21-26, 2003 (in Japanese).
29) Ochiai, T. and Enomoto, T.: Analysis on Predominant Periods Distribution by Microtremor Observations for Seismic Disaster Prevention in Yokohama, Japan Using GIS, *Journal of Geographic Information System*, Vol. 11, pp. 579–594, 2019.
30) Yokohama City Institute of Environmental Science: Yokohama City Ground Environment Investigation Report, 243 pp., 2003 (in Japanese, title translated by the authors).
31) Yokohama City General Affairs Bureau: Strong Motion Network, 2022 (in Japanese, title translated by the authors). http://www.city.yokohama.lg.jp/somu/org/kikikanri/eq/. (last accessed on February 2, 2022)
32) National Research Institute for Earth Science and Disaster Resilience: NIED K-NET, KiK-net, National Research Institute for Earth Science and Disaster Resilience, 2019. DOI: https://doi.org/10.17598/NIED.0004
33) The Headquarters for Earthquake Research Promotion: Modeling of the Subsurface Structure in Kanto Area ver.2017, 61 pp., 2017 (in Japanese, title translated by the authors). https://www.jishin.go.jp/evaluation/strong_motion/underground_model/integration_model_kanto (last accessed on February 2, 2022)

(Original Japanese Paper Published: November, 2021)
(English Version Submitted: February 3, 2022)
(English Version Accepted: March 27, 2022)